Microstructure of Directionally Solidified Ti-52Al-2W-0.5Si Intermetallic

T. Cheng[1,2], A. Mitchell[1], J. Beddoes[2], L. Zhao[3] and S. Durham[4]

[1]*Dept. of Met. & Mat. Engineering, University of British Columbia, Vancouver, Canada,*
[2]*Dept. of Mech. & Aero. Engineering, Carleton University, Ottawa, Canada,*
[3]*Structures, Materials & Propulsion Lab., Institute for Aerospace Research, National Research Council, Ottawa, Canada,*
[4]*Pratt & Whitney Canada Inc., Longueuil, Canada*

(Received July 22,1999)

ABSTRACT

The phase transformations controlling the microstructural evolution during directional solidification (DS) using the Bridgeman process and subsequent cooling are described for a Ti-52Al-2W-0.5Si intermetallic. The DS structure consists mainly of columnar dendrites with various shapes. α-Ti with a dendritic morphology is the primary solidified phase, followed by an incomplete peritectic reaction liquid (L)+α → γ-TiAl. The remaining liquid solidified as γ and silicides. During cooling after solidification α dendrites transform into ordered α_2 and γ with various morphologies, including near fully lamellar, script α_2 in a γ matrix and blocky α_2 in a γ matrix. Very fine tungsten-rich precipitates are also observed. The DS alloy is quite brittle. The microstructural evolution and the reason leading to the brittleness of the alloy are discussed.

1. INTRODUCTION

Interest has been focused on intermetallic TiAl as a most promising candidate material for replacement of conventional high temperature alloys, such as nickel-based superalloys. Among various types of TiAl intermetallics, two phase α_2-Ti3Al and γ-TiAl lamellar structures have received attention due to their potential to achieve balanced mechanical properties at both elevated and room temperatures /1-3/. The mechanical properties of these two-phase TiAl intermetallics are dependent on microstructural parameters, such as shape, size, distribution and relative content of each phase. Likewise these factors are influenced by composition, fabrication processing and possible heat treatment and thermal mechanical processing of the alloy. However, a complete understanding of the lamellar structure that would allow accurate control of the microstructure is lacking, particularly at elevated temperatures and when compositions contain multiple alloying elements.

Various fabrication processes including casting, casting followed thermal mechanical treatment, powder metallurgy and directional solidification (DS) have been applied to TiAl /3,4/. DS processing has been successfully used for industrial production of many superalloys to produce aligned crystals, which are normally parallel to the external stress direction /5/. Considerable effort /3,6-12/ has been focused on a similar route for making TiAl alloys. A floating zone melting technique has been used for most of this work /3,6-10/ partly due to the difficulty of dealing with the very reactive nature of molten titanium. Consequently, the size of DS bars produced is limited, and the slow solidification rate reduces the economic feasibility. In contrast, Bridgeman processing /5/ is capable of producing much larger DS bars and is potentially scaleable to industrial production.

In addition to the foregoing, examination of DS processed microstructures may provide information that advances the understanding of TiAl solidification behaviour. Hence, some research effort has concentrated

on Bridgeman processing of TiAl intermetallics /11-13/, focusing mainly on titanium-rich compositions. Regarding DS aluminum-rich TiAl, only binary alloys (Ti-52~56Al) fabricated by the floating zone melting technique have been studied /6,7,10/.

In the present work, an aluminum-rich DS Ti-52Al-2W-0.5Si (atomic percent) has been made by Bridgeman processing to study the effects of aluminum content and alloying additions on microstructures of the DS alloy. The DS structure and phase morphology, including various $\alpha_2+\gamma$ structures have been evaluated. The solidification sequence and solid state evolution of the phases have been analyzed. The possible relationship between microstructure and mechanical properties of the intermetallic is discussed.

2. EXPERIMENTAL

Investment cast master alloy bars of Ti-52Al-2W-0.5Si were DS processed in a Bridgeman furnace of the type illustrated in Figure 1, to produce bars of 95-135 mm length and 19-22 mm diameter, such as shown in Figure 2. The withdrawal rate or growth rate of the DS bars was 3 mm/min. An atmosphere of flowing high purity argon was maintained in the furnace during melting and solidification.

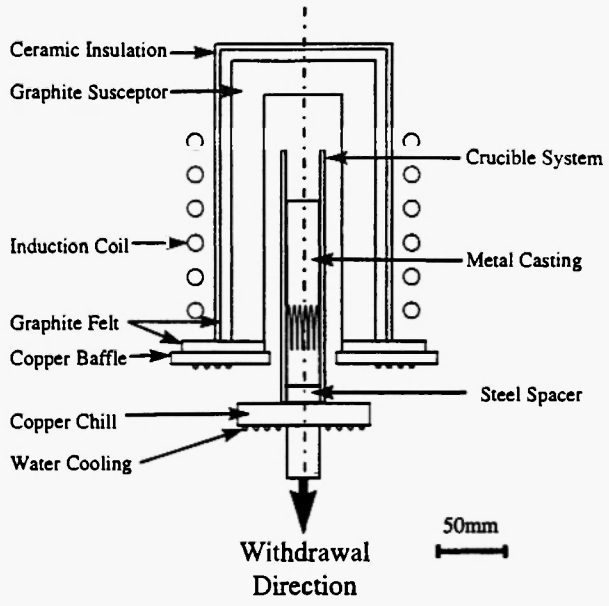

Fig. 1: Schematic drawing of a Bridgeman DS furnace used to make T-52Al-2W-0.5Si alloy.

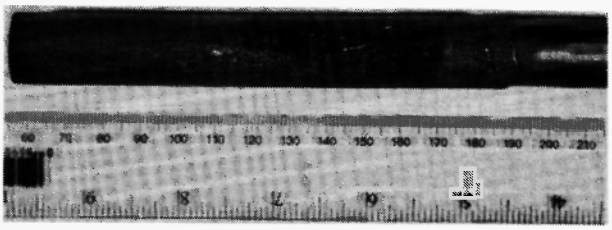

Fig. 2: DS bar made by Bridgeman processing (not etched).

The DS bar was longitudinally cut into halves by EDM (electric discharge machining). The microstructures of longitudinal sections were analyzed by optical microscopy and scanning electron microscopy (SEM). Microanalysis of the composition was determined by means of energy dispersive spectroscopy (EDS), with a consistency within about 0.5at% for the elements in the current composition.

3. RESULTS

3.1 DS structure

As shown in Figure 3, the DS structure consists of three parts. The top and middle portions of the bar exhibit well developed columnar dendrites basically parallel to the growth direction (the region 'P' of Figure 3). A few dendrites oriented at about 45° to the longitudinal axis of the bar exist in the upper portion of the region 'P'. Below the region 'P' are radial columnar dendrites normal to the surrounding surface (the region 'R' of Figure 3). Nearly equiaxed grains are present near the bottom of the melted part of the DS bar (the region 'E' of Figure 3). Figure 4 illustrates each of these regions at higher magnification. The regions identified as 'E' and 'R' are associated with the initial solidification transient and high undercooling, before stable steady state heat transfer during withdrawal is established. The region 'P' is the major part of the bar corresponding to stable growth. Region 'P' accounts for approximately 70% of the length of the bars produced. This DS structure is similar to that of concurrent work /14/, and previous studies /11-13/ on DS titanium-rich

Fig. 3: Longitudinal section of DS bar at low magnification (etched, "P": parallel columnar dendrite to growth direction, "R": radial columnar dendrite, "E" nearly equiaxed grains).

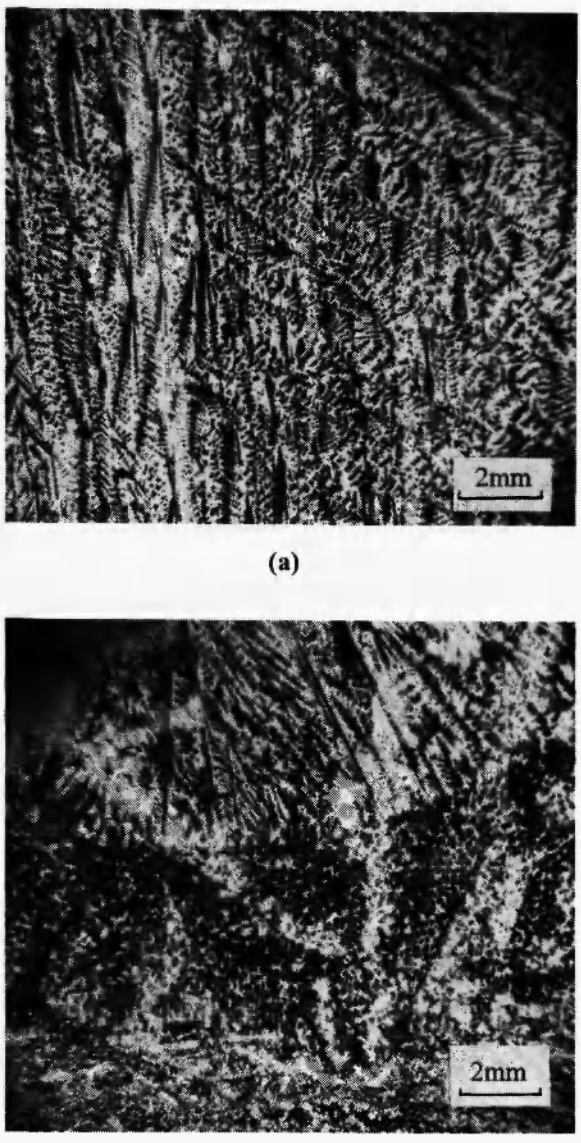

Fig. 4: Three parts in DS structure (optical micrographs) (a) parallel columnar dendrite (b) radial columnar dendrite and nearly equiaxed grains.

TiAl alloys produced via Bridgeman processing, except that the columnar dendrites are more developed in the current alloy.

3.2 Phase Structure

Only the binary Ti-Al phase diagram is available. However, it was reported /15/ that the alloying additions did not significantly alter the phases from those of the binary phase diagram. Hence, a high temperature part of a pseudo binary Ti-Al phase diagram /4/ (Figure 5) is used as the basis for the following analysis.

From Figs.6 and 4(a) it can be seen that the dendrites show six-fold symmetry Combined with information

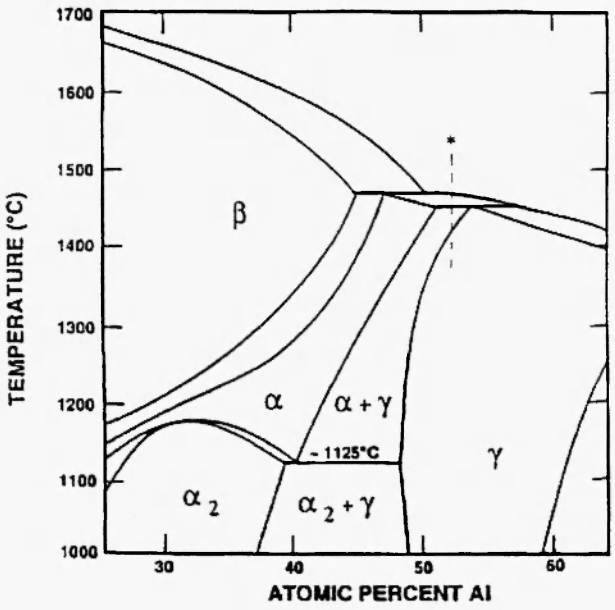

Fig. 5: A high temperature part of Ti-Al pseudo binary phase diagram /4/ (dotted line indicates the current alloy).

Fig. 6: Optical micrograph of parallel columnar dendrites at larger magnification, arrows point to peritectic γ phase (γ_P).

from the binary phase diagram (Figure 5), it can be deduced that these dendrites are primary α. Many dendrites are surrounded by a narrow enveloping phase as shown in Figure 6, which is normally a sign of a peritectic reaction. Based on the composition and phase diagram, the envelope phase should be γ (γ_P in Table I).

The microstructure of Figure 4(a) contains about 40 volume percent of interdendritic matrix, with a greater aluminum content than γ_P, suggesting that the matrix phase is also γ phase (γ_I in Table I), consistent with the

Table 1

The composition of major phases and structures (at%)

Phase or Structures	Al	Ti	W	Si
Dendrite envelope phase (γ_P)	55.2	42.5	2.3	
Interdendrite matrix (γ_I)	57.0	41.5	1.5	
Average Dendrite Composition				
Near Fully Lamellar Dendrites Fig. 7(a)	52.1	45.0	2.9	
Script Morphology Dendrites, Fig. 7(b)	52.7	44.5	2.8	
Duplex Dendrites, Fig. 7(c)	53.1	44.3	2.6	
Dendritic Phase Compositions				
Wide lamellae of Fig. 7(a) (γ_A)	53.2	44.1	2.7	
Narrow lamellae of Fig. 7(a) (α_2)	51.0	46.2	2.8	
Matrix of Fig. 7(b) (γ_B)	53.9	43.6	2.5	
Script phase of Fig. 7(b) (α_2)	51.8	45.6	2.6	
Matrix of Fig. 7(c) (γ_C)	53.3	44.0	2.7	
Blocky phase of Fig. 7(c) (α_2)	47.9	49.3	2.8	
Dendritic W-rich Compound	25.4	42.1	32.5	
Silicides Figure 8(a)	14.9	50.6	3.1	31.4
Silicide Figure 8(b)	21.7	51.6	3.1	23.6

expectation from the phase diagram (Figure 5). Together the γ_P and γ_l phases give a total γ volume fraction of about 45%.

The microstructure within the α dendrites is complicated. Based on their morphology the dendrites can be divided into three types with (A) a near fully lamellar structure, Figure 7(a), (B) precipitates with a script morphology, Figure 7(b), and (C) a two phase

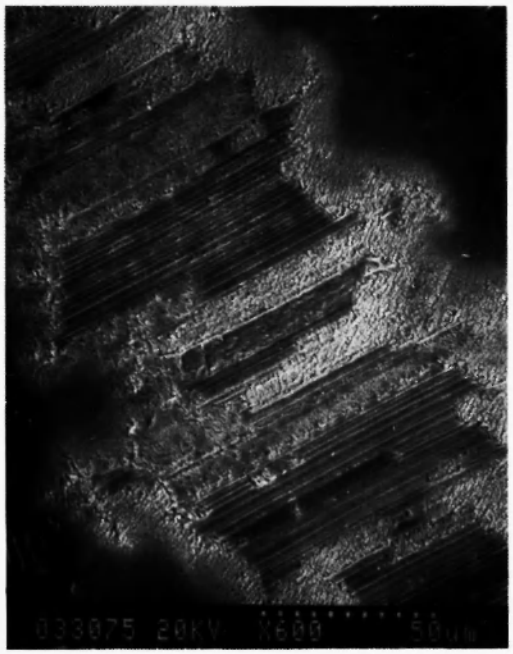

(a)

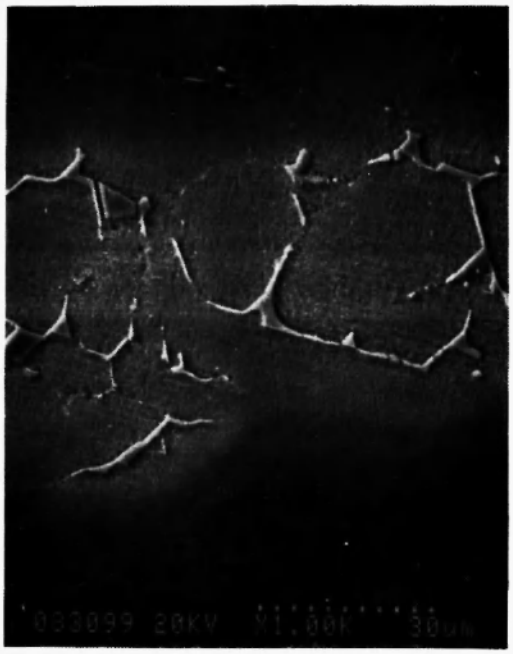

(b)

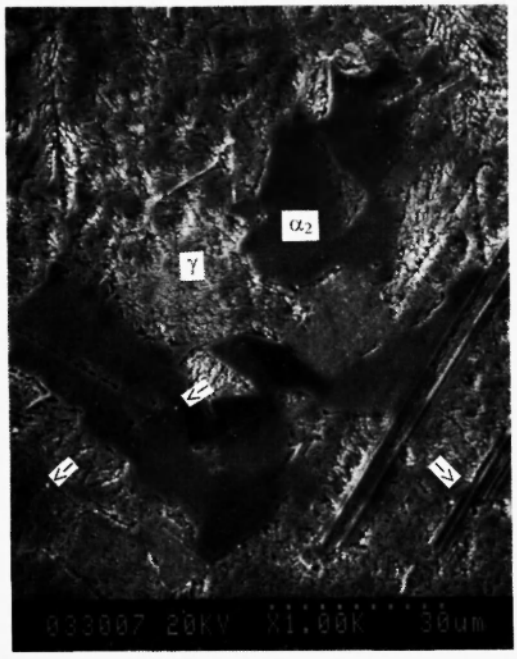

(c)

Fig. 7: Three types of structures within dendrites (SEM micrographs). (a) nearly full lamellar, (b) script precipitates on a matrix, (c) two-phase duplex dendrite structure, (d) EDS pattern of the tungsten-rich particles indicated by arrows in (c).

Fig. 7: continued...

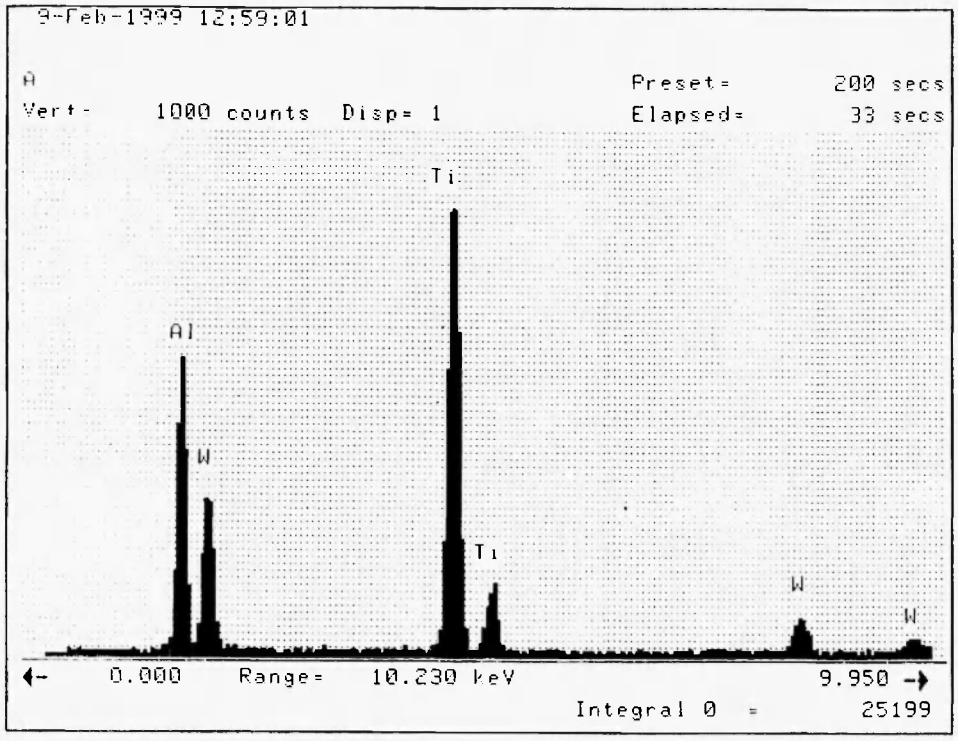

(d)

duplex structure, Figure 7(c). The average composition of each region, measured by EDS, is listed in Table I. According to the compositional analysis and phase diagram of Figure 5, the dendrites of all three types consist of γ matrix ($\gamma_{A\ to\ C}$ in Table I) and α_2 phase. The major differences among the three types of dendrites are the shape and content of the α_2 phase. In the near fully lamellar structure, Figure 7(a), groups of $\alpha_2 + \gamma$ lamellae are separated γ regions. In Figure 7(b) the script α_2 grew with certain orientations, with the α_2 increasing in thickness at the junction of each orientation, suggesting that the α_2 may nucleate from the junctions. In the duplex morphology, Figure 7(c), blocky α_2 is distributed within a γ matrix, with small lamellar regions also present. In addition, a very fine particle can be found within dendrites, mainly in dendrites with the duplex morphology, Figure 7(c). Qualitative EDS analysis of the fine particles indicates tungsten enrichment, Figure 7 (d). The formation and evolution of the dendrites is discussed later.

Two kinds of silicides (Figure 8) were found in the interdendritic γ_1 matrix. The silicides of Figure 8(a), with nearly round or extended round shape and smaller size (about 1-5 μm), contain more silicon than those with an extended shape and larger size (up to about 40 μm), Figure 8(b). The ratio of titanium to silicon in the former is close to Ti_5Si_3, which was observed in DS Ti-Al-Si /16/, but the silicide in the current alloy contains additional aluminum and tungsten. Both types of silicides form clusters within the γ matrix. The distance between the silicide clusters of Figure 8(a) is nearly homogeneous, suggesting that these may form from a eutectic reaction with the nearby γ phase.

The alloy of the current investigation is brittle and some microcracks formed during grinding and polishing, an example of which is illustrated in Figure 9.

(a)

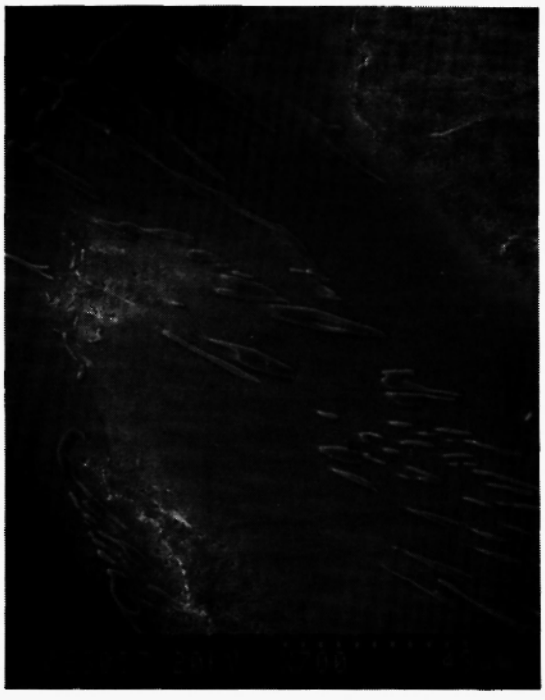

(b)

Fig. 8: Silicides in the inter-dendrite matrix (SEM micrographs) (a) with nearly round shape and smaller size and (b) with extended shape and larger size.

Fig. 9: Microcracks initiated along a group of silicides in inter-dendrite matrix (SEM micrograph).

4 DISCUSSION

4.1 Solidification sequence

Based on the experimental results and the pseudo Ti-Al phase diagram (Figure 5), a peritectic reaction $L+\alpha \rightarrow \gamma_P$ should follow the solidification of the primary α phase. However, it is clear this reaction is not complete. The α phase was entirely transformed into γ_P only in narrow parts of the dendrites. In other areas the peritectic reaction formed a surrounding envelope, with some parts of the dendrites not involved in the peritectic reaction. In fact, as indicated by the phase diagram, when the primary α dendrite forms with less aluminum than the average composition of the alloy it must reject more aluminum to the nearby liquid. Thus, it is possible for the aluminum content of the inter-dendrite liquid to be locally greater than the peritectic liquidus, causing this liquid to solidify directly as γ_l matrix, leaving the nearby α dendrite unaffected. In the majority of the cast bar, following the peritectic reaction the remaining liquid solidified as γ_l with silicide formation at the end

of the solidification process. Consequently, the solidification sequence can be summarized as:

$$L \rightarrow L+\alpha \rightarrow L+\alpha+\gamma_P \rightarrow \alpha+\gamma_P+\gamma_I + \text{silicides}$$

The solidification morphology in the current alloy is quite different from that in DS binary alloy with a similar aluminum content. A banded structure consisting of alternative layers of single γ phase and $\alpha_2+\gamma$ lamellar structure transformed from α was respectively found in DS Ti-52Al and Ti-54Al /3,7/. The large equilibrium partition coefficient and alternative rejection of more solute or solution element into the melt after local solidification was used to explain the solidification microstructure. However, this previous work was done at very slow growth rates, *R*, 10 mm/h /7/ and 5 mm/h /3/, in comparison with 3 mm/min (equivalent to 180 mm/h) for the current work. If the temperature gradient, *G*, in all of this work does not vary widely, the lower *R* (about 1/20-1/30 of that for the current work) would make the value of *G/R* larger. It is well known that a larger *G/R* would favour stability of the solid/liquid interface /17/. Consequently, planar solidification occurred in the previous work /3,7/, but the current alloy solidified mainly with a dendritic structure. In terms of adjusting the composition ahead of the solid/liquid interface to the required composition of the next solidified phase, the non-planar interface has higher interface density, and is, therefore, more efficient than a planar interface in this regard. The dendrite α and γ_I matrix may be viewed as a kind of incomplete band structure. The alloying additions of tungsten and silicon may also affect the equilibrium partition coefficient so as to affect the solidification morphology.

By comparing the solidification sequence with the binary phase diagram, it appears that the high temperature part of the binary phase diagram, shown in Figure 5, is not markedly affected by the addition of W and Si. However, the percent content of γ phase and the compositions corresponding to the peritectic solidus (51at%Al) and liquidus (55at%Al) /10/ in binary Ti-Al phase diagram are changed by the alloying additions. According to the lever rule and the two peritectic compositions, the γ_I matrix and γ_P envelope phases should account for about 30% volume fraction, which is consistent with the estimation in binary Ti-52Al alloy /7/, instead of the 45% of the current structure.

4.2 Dendritic $\alpha_2+\gamma$ structure

According to the phase diagram (Figure 5) the dendritic α phase in a binary Ti-52at%Al should transform to a single γ phase after solidification. However, it was reported /18/ that tungsten is a strong β stabilizer. It is possible that the phase boundary between $(\alpha+\gamma)$ and γ and between $(\alpha_2+\gamma)$ and γ in the current alloy is shifted to higher aluminum contents. This would allow α to transform to $\gamma+\alpha$ or $\gamma+\alpha_2$ during cooling. The results shown in Figure 7 and mentioned in 3.2 are consistent with these suggested transformations. Additionally, as shown in Figure 7, three different $\alpha_2+\gamma$ dendritic morphologies are present in the current DS alloy, with no correlation to the location of the dendrite in the DS bar.

During the cooling the primary α phase first precipitates γ when it enters the $(\alpha+\gamma)$ two-phase region. For the current alloy the γ phase would become the major phase as the eutectoid temperature is approached, with its relative content changing little during cooling from the eutectoid to room temperature due to the negative slope of the boundary between γ and $\gamma+\alpha_2$ regions. To satisfy the requirements of minimum thermodynamic free energy, not only is redistribution of aluminum/ titanium atoms required, but also the change of crystal structures from hexagonal to tetragonal and the change from disordered to ordered structure must be completed. Although the cooling rate is quite slow during DS processing, it appears that the time was not kinetically sufficient to complete the changes during the cooling for the near fully lamellar dendritic structures, Figure 7(a). Consequently, the distribution of α or α_2 within the γ matrix is not homogeneous, with some regions containing only the γ matrix.

The orientation of the α_2 phase with script morphology in dendrites, Figure 7(b), may relate to the habit planes for the initial formation of γ from α phase. The duplex dendrites, Figure 7(c), contain blocky α_2 and γ, likely as a result of longer range diffusional reaction than those producing the dendrites with near lamellar morphology. It is well established that cooling rate from the α region through the $(\alpha+\gamma)$ region influences the morphology of the resultant $\alpha/\alpha+\gamma$

microstructure, with the lamellar structure kinetically more favorable than script or duplex structures. In the current material, it is postulated that segregation or small differences in the local composition of the α – especially due to an inhomogeneous distribution of tungsten – causes different transformation kinetics leading to the three dendritic morphologies of Figure 7. Although the compositional differences of the three types of the dendrites, Table 1, are on the limit of EDS resolution, the differences detected are consistent with the foregoing postulation.

Further research to investigate the formation and evolution of the dendritic structures is required to completely understand the possible transformation pathways.

4.3 Lamellar orientation

To enhance both elevated and room temperature mechanical properties, a major concern of previous research has been the development of a fully lamellar DS TiAl structure with the lamellae parallel to the growth direction /3/. However, almost all lamellae in the dendrites of the current alloy have an angle of 45-90° to the growth direction as typically shown in Figure 6. Johnson *et al.* /8/ discussed the relationship between lamellar orientation and primary phase during solidification. According to their considerations, when α is the primary phase during solidification, its preferred growth direction is [0001]. During the subsequent solid state transformation $\alpha \rightarrow \gamma$, the orientation relationship is $(0001)_\alpha // (111)_\gamma$ and $<1120>_\alpha // <110>_\gamma$. The boundaries of subsequent α_2/γ lamellae would all be perpendicular to the growth direction. Hence, they suggested changing the primary phase from α to β to achieve the ideal microstructure. Compared with the current experimental results, the considerations of Johnson *et al.* are, at least, partially correct since no lamellar structure aligned in the growth direction has been found. However, as shown in Figure 6, many lamellar boundaries are not perpendicular to the growth direction. Also observed are additional features in other DS alloys /14/, which can not be explained by their analysis. In addition, it is noted in their recent published work on DS Ti-Al-Mo-B /13/, that although β was the primary phase, only a small portion of columnar grains had lamellae parallel to the growth direction. It is clear that lamellar alignment is a complicated issue not only associated with solidification reactions, but also with subsequent solid state transformations. The lamellar orientation is the subject of continuing research.

4.4 Possible reasons for brittleness

As shown in Figure 8, the large silicides and clustering of silicides close to the relatively less ductile dendrites containing the α_2 phase certainly contributes to the brittleness of the current alloy. Particularly, a cluster of brittle silicides, normally about 50-70 μm in size, is approximately equivalent to a large brittle inclusion. Thus microcracks could easily nucleate around the interface between silicides and the γ matrix when an external stress is applied. Figure 9 shows an example, in which a microcrack started to form associated with a silicide cluster, supporting this analysis.

The other contribution to brittleness is the high aluminum content. It is known that tensile ductility is quickly reduced to zero when the aluminum content exceeds the stoichiometric ratio /10/. Furthermore, the addition of tungsten may have a negative effect on the ductility of the current alloy. Some microcracks observed in the alloy do not have any direct link to the silicides and traverse both dendritic and matrix regions, suggesting inherent brittleness, regardless of the silicides.

5. CONCLUSIONS

(1) DS Ti-52Al-2W-0.5Si exhibits a DS structure that includes parallel columnar dendrites to the growth direction as the major part of the DS bar, radial columnar dendrite and near equiaxed grains.

(2) The primary solidification phase is α with a dendritic morphology, followed by an incomplete peritectic reaction between liquid and α to produce a γ envelope surrounding many dendrites. The last solidified phases are interdendrite γ matrix and silicides.

(3) The α dendrite undergoes solid state transformations into γ and α_2 during the cooling with three

morphologies. The reason for the various morphologies needs to be further investigated.

(4) There are two kinds of silicides with different size and silicon content within the interdendrite γ matrix. The silicides tend to form clusters close to dendrites. Small tungsten-rich particles are mainly located within the dendrite, and probably form by precipitation.

(5) The DS Ti-52Al-2W-0.5Si alloy is brittle. The silicides and higher aluminum content may be the major contributors to brittleness.

ACKNOWLEDGEMENTS

This research was completed with the financial support of the Natural Science and Engineering Research Council and National Research Council *Research Partnership Program*. Industrial funding was contributed by Pratt & Whitney Canada, Inc. The authors are grateful to these organizations for the opportunity to undertake the research described.

REFERENCES

1. Y-W. Kim, *JOM*, **6**, 43 (1994).
2. Y-W Kim and D. Dimiduk, *Structural Intermetallics*, M.V. Nathal, R. Darolia, C.T. Liu, P.L. Martin, D.B. Miracle, R. Wagner and M.Yamaguchi (Eds.), TMS, 531 (1997).
3. D.R. Johnson, Y. Masuda, Y. Shimada, H. Inui and M. Yamaguchi, *Structural Intermetallics*, M.V. Nathal, R. Darolia, C.T. Liu, P.L. Martin, D.B. Miracle, R. Wagner and M.Yamaguchi (Eds.), TMS, 287 (1997).
4. L. Semiatin, J.C. Chesnutt, C. Austin and V. Seetharaman, *Structural Intermetallics*, M.V. Nathal, R. Darolia, C.T. Liu, P.L. Martin, D.B. Miracle, R. Wagner and M.Yamaguchi (Eds.), TMS,, 263 (1997).
5. M. McLean, *Directionally Solidified Materials for High Temperature Services*, The Metals Society, London, 1983.
6. B.F. Oliver, B.Y. Huang and W.C. Oliver, *Scripta Metall.*, **22**, 1405 (1988).
7. Y.J. Bi and J.S. Abell, *Scripta Metall. Mater.*, **31**, 751 (1994).
8. M. Kim, M. Oh, D. Wee, H. Inui and M. Yamaguchi, Mater. *Trans., JIM*, **37**, 1197 (1996).
9. D.R. Johnson, Y. Masuda, H. Inui and M. Yamaguchi, *Acta. Mater.*, **45**, 2523 (1997).
10. D.R. Johnson, H. Inui and M. Yamaguchi, *Intermetallics*, **6**, 647 (1998).
11. B. London, D.E. Larsen Jr., D.A. Wheeler and P.R. Aimone, *Structural Intermetallics*, R. Darolia, J.J. Lewandowski, C.T. Liu, P.L. Martin, D.B Miracle and M.V. Nathal (Eds.), TMS, 151 (1993).
12. D.R. Johnson, Y. Masuda, H. Inui and M. Yamaguchi, *Mater. Sci. Eng.*, **A239-240**, 577 (1997).
13. D.R. Johnson, K. Chihara, H. Inui and M. Yamaguchi, *Acta Mater.*, **46**, 6529 (1998).
14. T. Cheng, A. Mitchell, J. Beddoes, L. Zhao, H. Saari and S. Durham, to appear in *High Temperature Materials and Processes*, 2000.
15. Y-W Kim, *Acta. Metall. Mater.*, **40**, 1121 (1992).
16. D.R. Johnson, H. Inui and M. Yamaguchi, *Acta Mater.*, **44**, 2523 (1996).
17. R. Chalmers, *Principles of Solidification*, John Wiley & Sons, NY, 1964.
18. S. Naka, M. Thomas, C. Sanches and T. Khan, *Structural Intermetallics*, M.V. Nathal, R. Darolia, C.T. Liu, P.L. Martin, D.B. Miracle, R. Wagner and M.Yamaguchi (Eds.), TMS, 313 (1997).